

## Preparation of High Tap Density LiFePO<sub>4</sub>/C through Carbothermal Reduction Process Using Beta-Cyclodextrin as Carbon Source

Yina Wu, Le Zhou, Guoqing Xu, Jie Huang, Xiong Fang, Yang Wang, Yuan Jin, Xincun Tang \*

College of Chemistry and Chemical Engineering, Central South University, Changsha 410083, China

\*E-mail: [tangxincun@163.com](mailto:tangxincun@163.com)

Received: 30 October 2017 / Accepted: 12 January 2018 / Published: 5 February 2018

---

As an economical and practical manufacturing process, the carbothermal reduction method is widely used for industrial production of LiFePO<sub>4</sub>. In this work, an LiFePO<sub>4</sub>/C cathode material with a high tap density of 1.3 g cm<sup>-3</sup> was successfully synthesized through a novel carbothermal reduction process, which used FePO<sub>4</sub> as the precursor and beta-cyclodextrin as the carbon source. The prepared samples were characterized by X-ray diffraction (XRD), X-ray photoelectron spectroscopy (XPS), scanning electron microscopy (SEM), transmission electron microscopy (TEM) and Raman spectra. Their electrochemical performance was investigated with a galvanostatic charge/discharge system, cyclic voltammetry (CV) and electrochemical impedance spectroscopy (EIS). The SEM and TEM results indicate that LiFePO<sub>4</sub>/C microspheres with diameters of 5-10 μm aggregated by enormous nanoplates, and they were evenly coated with an amorphous carbon layer approximately 3 nm thick. The electrochemical results show that carbon coating could greatly optimize the electrochemical performance of LiFePO<sub>4</sub> owing to the improved electronic conductivity of the sample. Specifically, LiFePO<sub>4</sub>/C exhibited not only a discharge capacity of 144 mAh g<sup>-1</sup> in the initial cycle at 0.1C (1C=170 mAh g<sup>-1</sup>), but also a superior rate capability and excellent cycling performance.

---

**Keywords:** LiFePO<sub>4</sub>/C; beta-cyclodextrin; carbothermal method; electrochemical performances

### 1. INTRODUCTION

With the rapid development of large-scale energy storage applications in recent years, such as electric vehicles (EV) and the smart grid, there is a growing demand for rechargeable batteries with greater energy density and better cycling stability [1, 2]. Compared with other traditional secondary batteries, lithium-ion batteries are more suitable for EV applications due to their high energy capacity and long life [3, 4]. In a lithium-ion battery system, the cathode material is one of the key factors

affecting the performance. Because the cathode influences on the cell voltage and cell capacity, the energy density and power density of lithium-ion batteries are mostly determined by the cathode material. Among these commercial cathode materials for lithium-ion batteries, lithium iron phosphate ( $\text{LiFePO}_4$ ) has been attracting the most attention due to its excellent electrochemical properties as well as its low cost[5], excellent thermal stability[6] and environmental friendliness[7]. However, they still face the challenge of low volumetric specific capacity in practical applications as the result of the low tap density of  $\text{LiFePO}_4$  powder[8, 9].

According to previous reports, the tap density of  $\text{LiFePO}_4$  powder is closely related to its morphology and particle size, and thus, much effort has been devoted to increasing the tap density through controlling the morphology and size distribution of  $\text{LiFePO}_4$  particles. For example, Sun synthesized  $\text{LiFePO}_4$  microspheres consisting of nanoplates using a solvothermal process, and the tap density of flower-like microspheres reached approximately  $1.1 \text{ g cm}^{-3}$ [10]. Similarly, Su prepared  $\text{LiFePO}_4$  microspheres composed of many nanoparticles with a tap density of  $1.2 \text{ g cm}^{-3}$  via a hydrothermal method[11]. These morphological characteristics equip  $\text{LiFePO}_4$  microsphere electrodes with a higher volumetric energy density. However, as mentioned above, most of the reported  $\text{LiFePO}_4$  samples with high tap density were synthesized through high-temperature hydro/solvothermal methods, which are difficult to scale up for large-scale industrial applications due to the long synthesis time and high processing costs. Carbothermal reduction, in this regard, is a feasible and efficient synthesis method able to produce large amounts of  $\text{LiFePO}_4$ . In addition to improving the tap density, efficient carbon coating method should be explored to improve the electronic conductivity of  $\text{LiFePO}_4$  and to enable the  $\text{LiFePO}_4$  electrode with higher specific capacity and better rate performance. Cyclodextrin was used as a novel carbon source for the synthesis of  $\text{Li}_3\text{V}_2(\text{PO}_4)_3/\text{C}$  materials, and this process was expected to improve the electronic conductivity[12]. From the above points, there is an urgent need to develop a feasible and efficient synthesis method to improve the electrochemical performance of  $\text{LiFePO}_4$ .

In this work, sphere-like  $\text{FePO}_4$  constructed from enormous nanoplates was first synthesized through a template-free hydrothermal method at  $80 \text{ }^\circ\text{C}$  and used for the preparation for  $\text{LiFePO}_4$ . Then, the  $\text{LiFePO}_4/\text{C}$  microspheres with a high tap density of approximately  $1.3 \text{ g cm}^{-3}$  were successfully prepared through the carbothermal method. Beta-cyclodextrin was used as the carbon source, and the thermal analysis results indicate that its carbon residue was higher than other common carbon sources. We also proposed a reasonable preparation process involving a low-temperature hydrothermal reaction for the formation of  $\text{FePO}_4$  followed by a carbothermal process to obtain the  $\text{LiFePO}_4/\text{C}$ . Above all, the as-made  $\text{LiFePO}_4/\text{C}$  composite showed an excellent rate performance and stable cycling stability in lithium-ion batteries.

## 2. EXPERIMENTAL

### 2.1 Preparation of $\text{LiFePO}_4/\text{C}$

Micron-sized ferric phosphate ( $\text{FePO}_4$ ) spheres were synthesized by a low-temperature hydrothermal process. Ammonium ferrous sulfate hexahydrate ( $(\text{NH}_4)_2\text{Fe}(\text{SO}_4)_2 \cdot 6\text{H}_2\text{O}$ ), urea

(CO(NH<sub>2</sub>)<sub>2</sub>) and phosphoric acid (H<sub>3</sub>PO<sub>4</sub>) were used as Fe and P sources dissolved in 50 mL of deionized water. The mixture was transferred to a 100-mL Teflon-lined stainless autoclave and heated at 80 °C for 8 h in an air circulation oven. After cooling to room temperature, the precipitate was filtered by a G<sub>4</sub> sand filter funnel and washed three times with distilled water and ethanol. The precipitate was dried in an oven at 80 °C for 8 h to obtain the precursor. A stoichiometric amount of precursor, lithium acetate dihydrate (LiAc·2H<sub>2</sub>O) and beta-cyclodextrin (C<sub>42</sub>H<sub>70</sub>O<sub>35</sub>) was used as the carbon source to synthesize samples. The combinations were mixed by ball-milling at 350 rpm for 2 h, and they were then heated at 700 °C for 10 h in a mixed hydrogen-argon atmosphere (5% H<sub>2</sub>+95% Ar). Finally, LiFePO<sub>4</sub> and LiFePO<sub>4</sub>/C were obtained via the above processes.

## 2.2 Material characterizations

The crystalline phase and composition of the prepared materials were detected by powder X-ray diffraction (XRD, Dandong Haoyuan, DX-2700) and X-ray photoelectron spectroscopy (XPS, ESCALAB250). The morphology and microstructure of the particles were investigated by scanning electron microscopy (SEM, Sirion 200) and high-resolution transmission electron microscopy (HRTEM, Tecnai F30). A Labram-010 laser Raman spectrometer was employed to obtain the Raman spectrum of LiFePO<sub>4</sub>/C. The BET (Brunner-Emmet-Teller) specific surface area and the N<sub>2</sub> adsorption-desorption isotherms were measured by N<sub>2</sub> adsorption-desorption method at liquid nitrogen temperature on an SSA-4000 instrument. The thermogravimetric curves were determined by a Netzsch STA 449C (Germany) at a heating rate of 10 °C min<sup>-1</sup>. The tap density of the LiFePO<sub>4</sub>/C powder was tested using the following method. A certain quantity of powder was weighed and added to a 5-mL dry cylinder, and then, the cylinder was tapped continuously until the volume of the powders no longer changed. The ratio of the quantity to the volume determines the tap density of the powders.

## 2.3 Electrochemical measurements

The cathode was prepared by mixing the LiFePO<sub>4</sub>/C, polyvinylidene fluoride (PVDF) binder and acetylene black with weight ratio of 80:10:10, the mixture was rolled into an aluminum-foil and then dried in a vacuum at 120 °C for 12 h. The thick sheet was cut into 1.2 cm in diameter and the typical electrode contained active materials approximately 2 mg. The coin cells were fabricated with a LiFePO<sub>4</sub> cathode, 1 M LiPF<sub>6</sub> in ethylene carbonate (EC)-dimethyl carbonate (DMC)-diethyl carbonate (DEC) (volume ratio of 1:1:1) electrolyte, a Celgard polypropylene separator, and metallic lithium foil anode in an argon-filled glovebox. The electrochemical performance of LiFePO<sub>4</sub> and the LiFePO<sub>4</sub>/C composite was tested using CR2016-coin cells between 2.5-4.2 V with a Neware battery testing system. The assembled cells were galvanostatically charged and discharged at various rates ranging from 0.1C to 5C. Cyclic voltammetry (CV) curves were recorded with a two-electrode set-up at a scan rate of 0.4 mV s<sup>-1</sup> at room temperature. Electrochemical impedance spectroscopy (EIS) was examined by applying an AC voltage of 5 mV with frequencies changing from 0.01 Hz to 100 kHz using a Zahner Elektrik potentiostat (IM6ex).

### 3. RESULTS AND DISCUSSION

To evaluate the level of residual carbon, different carbon sources (glucose, phenol-formaldehyde resin and beta-cyclodextrin) were analyzed through thermogravimetric (TG) measurements in an  $N_2$  atmosphere at a heating rate of  $10\text{ }^\circ\text{C min}^{-1}$ , and the TG curves are shown in Fig. 1a-c. The residue weight of glucose and phenol-formaldehyde resin is 6 wt.% and 15 wt.%, respectively, while beta-cyclodextrin with a high content of residual carbon reached as high as 20 wt.%. These results suggest that more carbon residue would be present in the  $\text{LiFePO}_4/\text{C}$  sample when using beta-cyclodextrin as a carbon source. Additionally, it is suitable to apply beta-cyclodextrin in a solid ball mill because it does not stick to the ball mill tank compared with glucose and phenol-formaldehyde resin; this is one of its advantages for its further application. It is essential for electrode materials to be coated with a suitable carbon source, and furthermore, different carbon sources have different coating effects on  $\text{LiFePO}_4$ . Coated carbon with a porous structure can promote the penetration of electrolyte into the electrode, which is mostly carbonized from a monosaccharide such as glucose and fructose. Meanwhile, another kind of coated carbon layer with a dense structure could contribute significantly to the electrical conductivity of the electrode materials, which is usually calcined from a macromolecular compound containing a benzene ring, such as phenol-formaldehyde resin. Beta-cyclodextrin is a kind of oligosaccharide encompassing seven glucose in a ring structure, and it contributes to the penetration of electrolyte and influences the electrochemical performance[13].

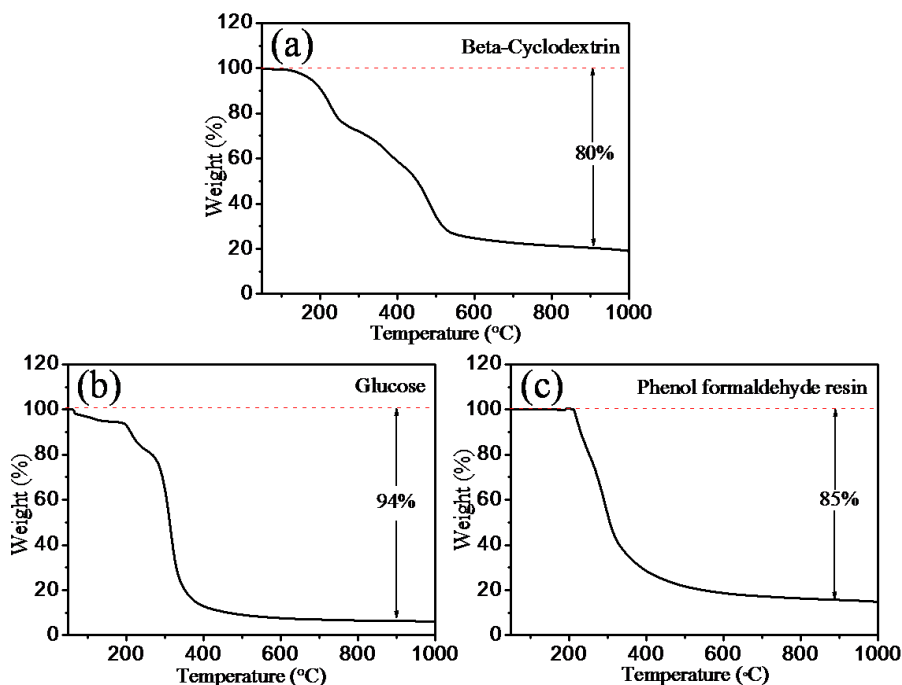


**Figure 1.** Thermogravimetry curves of (a) beta cyclodextrin, (b) glucose and (c) phenol-formaldehyde resin.

The crystal structure and phase composition of  $\text{FePO}_4$  and  $\text{LiFePO}_4/\text{C}$  microspheres were analyzed by XRD, and the X-ray diffraction patterns are shown in Fig. 2. For the  $\text{FePO}_4$  sample, there is no apparent diffraction peak in Fig. 2a, indicating that the as-made  $\text{FePO}_4$  precursor is amorphous.

Whereas, the main diffraction peaks of  $\text{LiFePO}_4/\text{C}$  sample testify a single phase of  $\text{LiFePO}_4$ , which can be indexed as the standard orthorhombic space group  $P_{mnb}$  62 (JCPDS No. 40-1499). The lattice parameters of  $\text{LiFePO}_4/\text{C}$  were determined to be  $a = 6.019 \text{ \AA}$ ,  $b = 10.347 \text{ \AA}$ ,  $c = 4.704 \text{ \AA}$ , which are close to the standard PDF card, indicating that carbon coating has no apparent influence on the structure. Moreover, the diffraction peaks are strong and narrow, and the peaks corresponding to impurity phases, which could decrease the electrochemical performance, such as  $\text{Li}_3\text{PO}_4$  and  $\text{Fe}_2\text{P}$ , are not present in Fig. 1b, revealing that the  $\text{LiFePO}_4/\text{C}$  products prepared were very pure and had high crystalline[14-16]. The results demonstrate that  $\text{LiFePO}_4/\text{C}$  was successfully generated from the  $\text{FePO}_4$  precursor,  $\text{LiAc}\cdot 2\text{H}_2\text{O}$  and beta-cyclodextrin.

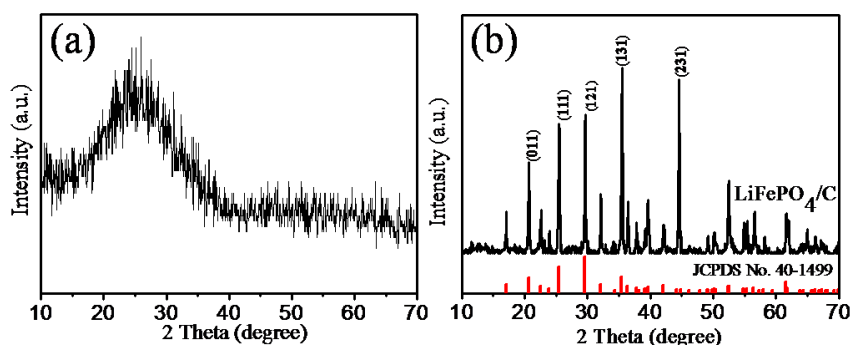


**Figure 2.** XRD patterns of  $\text{FePO}_4$  and  $\text{LiFePO}_4/\text{C}$ .

XPS analysis is one of the most practical techniques for detecting the elemental composition of the  $\text{LiFePO}_4/\text{C}$  sample and the oxidation state of Fe in  $\text{LiFePO}_4/\text{C}$ . The full-spectrum XPS and the XPS spectra at the binding energies of C 1s and Fe 2p are shown in Fig. 3a-c. As shown in Fig. 3a, the peaks corresponding to Fe, O, C and P can be observed, indicating the presence of Fe, O, C and P on the surface of the sample. It also implies that the thickness of the carbon layer was no more than 10 nm because the detection thickness of the X-rays in XPS can only reach to  $\sim 10$  nm, and this is verified by the results of the HR-TEM image (Fig. 4d)[17]. The peak of the C 1s line is found at 284.79 eV in Fig. 3b, which indicates the presence of amorphous carbon[18]. The Fe 2p spectrum consists of two main peaks and their satellite peaks shown in Fig. 3c. The Fe  $2p_{3/2}$  main peak appears at 710 eV with a satellite peak at 713.6 eV, and the Fe  $2p_{1/2}$  main peak is at 723.4 eV with a satellite peak at 727.4 eV. The spin-orbital split energy is 13.4 eV. The values are consistent with those of  $\text{Fe}^{2+}$ , revealing that the valence state of Fe is +2[19-21]. Meanwhile, the results reveal that  $\text{Fe}^{3+}$  was reduced to  $\text{Fe}^{2+}$  completely during the carbon thermal reduction process. The results further attest the feasibility of producing the  $\text{LiFePO}_4/\text{C}$  composite materials by carbothermal reduction based on beta-cyclodextrin as the carbon source.

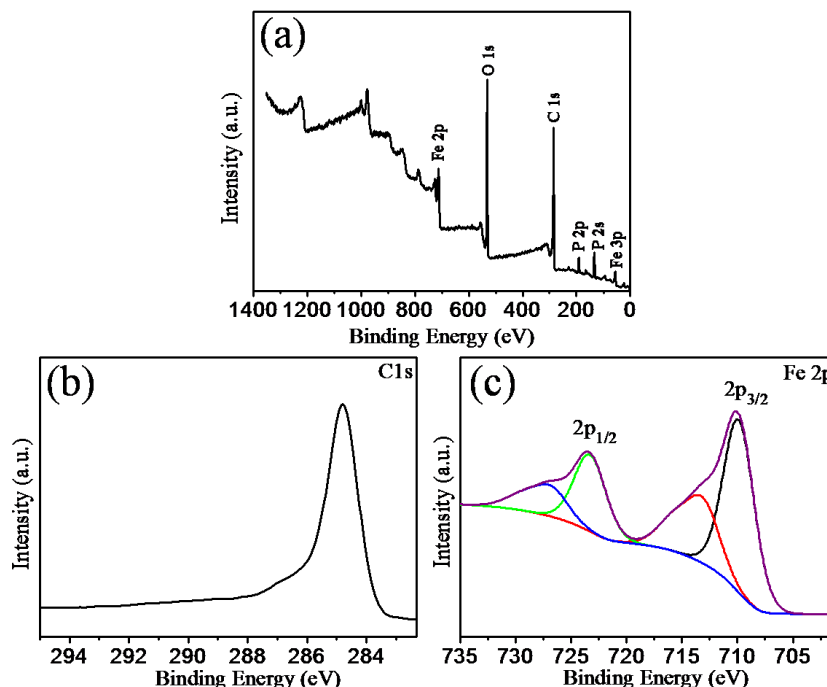


**Figure 3.** The full XPS spectra for LiFePO<sub>4</sub>/C; C 1s and Fe 2p core spectra for sample.

Scanning electron microscopy (SEM) images of FePO<sub>4</sub> and the LiFePO<sub>4</sub>/C microspheres are shown in Fig. 4a-b. A sphere-like morphology of FePO<sub>4</sub> is observed with fine and homogeneous particle size of approximately 5-10  $\mu\text{m}$  aggregated by enormous nanoplates. After the carbothermal reduction process, the particle size was changed slightly, while the surface of these porous particles obviously melted to produce LiFePO<sub>4</sub>/C; this may result from the carbonization of beta-cyclodextrin, which can tightly contact the bulk. This also made the tap density of the LiFePO<sub>4</sub>/C sample reach to 1.3  $\text{g cm}^{-3}$ , which is much higher compared with the values previously reported in the literature[10, 22, 23]. More details of the comparison are shown in Table 1, it can be seen that the tap density of micro-nano spherical LiFePO<sub>4</sub>/C prepared through carbothermal reduction method is highest. One of the major methods to satisfy the requirement of a high volumetric specific capacity is by improving the tap density of LiFePO<sub>4</sub>. To accurately analyze the porosity of the LiFePO<sub>4</sub>/C composites, N<sub>2</sub> adsorption-desorption isotherms and the corresponding Barrett-Joyner-Halenda (BJH) distribution of pore size are shown in Fig. 4c. These analyses illustrate a type-IV adsorption-desorption isotherm with H<sub>3</sub>-type hysteresis[24, 25]. The adsorption isotherm of LiFePO<sub>4</sub>/C shows a hysteresis loop, and the pore size distribution is concentrated with the average pore diameter of 7.5 nm calculated from the desorption branch of the nitrogen isotherm, indicating that the sample is a mesoporous material. The measured Brunauer-Emmett-Teller (BET) area is 44.1  $\text{m}^2 \text{g}^{-1}$ . The surface area may benefit from a porous structure of LiFePO<sub>4</sub>/C, as shown in Fig. 4b; the corresponding BJH desorption accumulative pore volume is 0.083  $\text{cm}^3 \text{g}^{-1}$ , which is still higher than that of previous literature reports[2, 26, 27]. The porous structure may better enable the penetration of electrolyte into the electrode materials to contribute to the rate performance of cathode material.

**Table 1.** Comparison between tap density of the LiFePO<sub>4</sub>/C with those in the literature.

Method	Morphology	Tap density (g·cm <sup>-3</sup> )	Ref
Co-precipitation	Spherical	1.0	[23]
Solvothermal	Flower-like	1.2	[10]
Hydrothermal	Microsphere	1.2	[22]
<b>Carbothermal reduction</b>	<b>Micro/nanospherical</b>	<b>1.3</b>	<b>This work</b>

To verify the crystal structure of LiFePO<sub>4</sub>/C and to determine the carbon distribution upon the particles, a high-resolution transmission electron microscopy (HRTEM) image and selected area electron diffraction (SAED) image were taken and are shown in Fig. 4d. The obvious lattice fringe and the diffraction spot in the alignment exhibit excellent single crystal character of the LiFePO<sub>4</sub>/C composite.

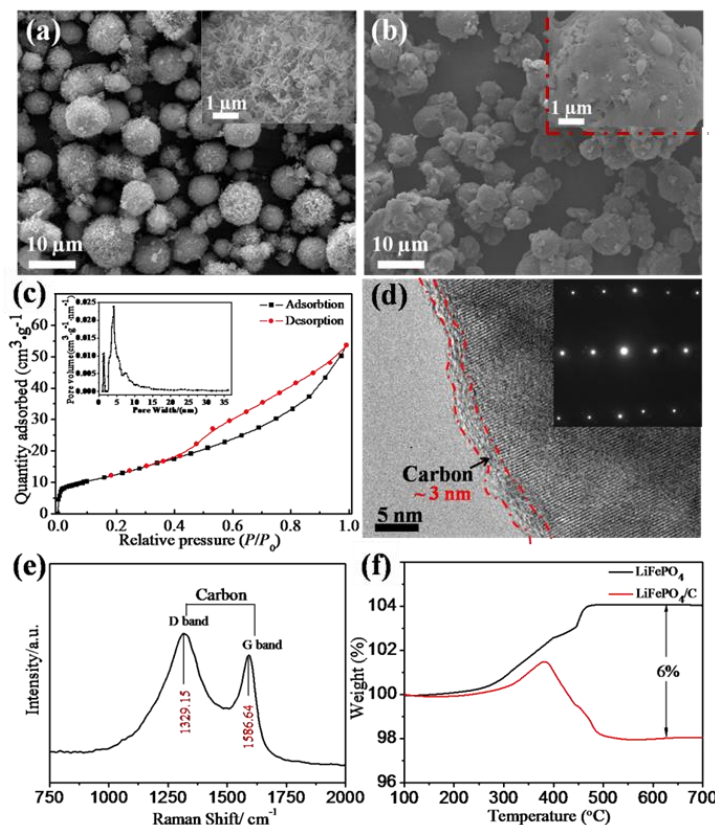
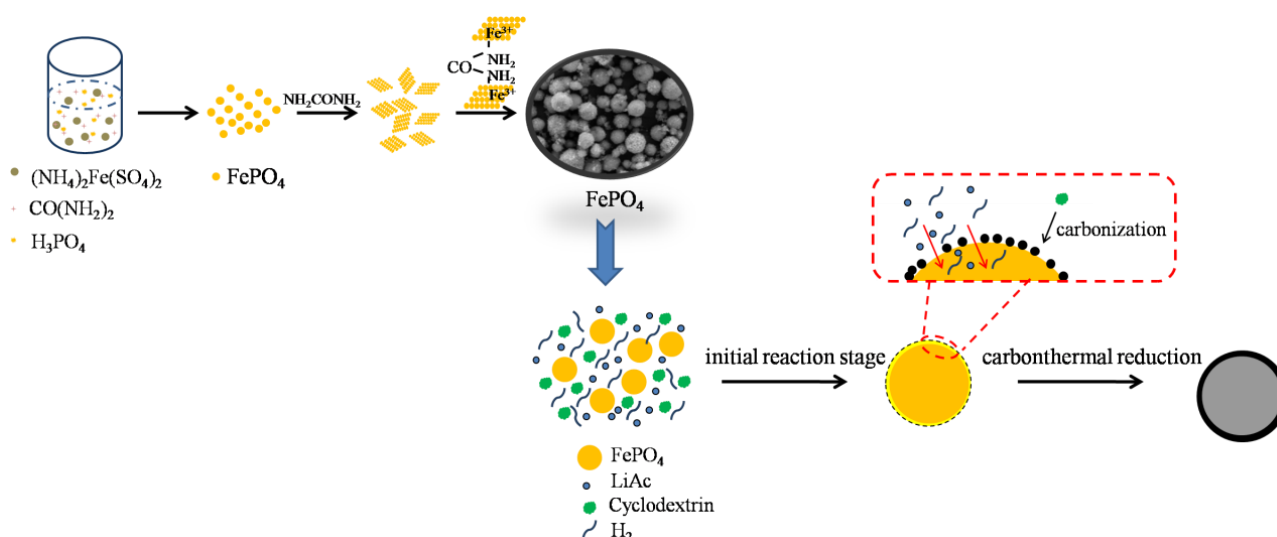


**Figure 4.** Scanning electron microscopic pictures of (a) FePO<sub>4</sub> and (b) LiFePO<sub>4</sub>/C; (c) the nitrogen adsorption-desorption isotherms and the BJH distribution of pore size images of LiFePO<sub>4</sub>/C. (d) TEM images and (e) Raman spectra of LiFePO<sub>4</sub>/C; (f) thermogravimetry curves of LiFePO<sub>4</sub> and LiFePO<sub>4</sub> samples. Inset in (d): SAED spot pattern

The surface of the  $\text{LiFePO}_4/\text{C}$  particles is coated with an amorphous carbon layer approximately 3 nm thick, which evenly formed from the decomposition of beta-cyclodextrin. The result is consistent with the analysis of XPS. The Raman spectrum in Fig. 4e was acquired to analyze the carbon composition. The spectrum clearly shows that the product displays two peaks at  $1329.15\text{ cm}^{-1}$  and  $1586.64\text{ cm}^{-1}$ , which belong to disordered carbon (D-band) and graphitic carbon (G-band), respectively[28, 29]. The Raman spectrum further confirms that most of the carbon exists in the amorphous phase, in accord with the results of the HRTEM. The existence of the carbon improves the electronic conductivity of the  $\text{LiFePO}_4$  particles and ensure a good electrical connection between the particles. The thermogravimetric (TG) curves of  $\text{LiFePO}_4$  and  $\text{LiFePO}_4/\text{C}$  were measured in air at a heating rate of  $10\text{ }^\circ\text{C min}^{-1}$  and are shown in Fig. 4f. Clearly, pure  $\text{LiFePO}_4$  gained a 4.0 wt.% weight increment, which is attributed to the oxidation of  $\text{Fe}^{2+}$ , while the as-prepared  $\text{LiFePO}_4/\text{C}$  loses up to 2.0 wt.% from the simultaneous oxidation of  $\text{Fe}^{2+}$  and C. These data indicate that the carbon content in the  $\text{LiFePO}_4/\text{C}$  can be estimated as 6.0 wt.% and demonstrate that a small amount of beta-cyclodextrin could generate abundant residual carbon after sintering.

According to the above results and analyses, we proposed a preparation process for  $\text{LiFePO}_4/\text{C}$ , which is schematically illustrated in Scheme 1. The first step was to synthesize spherical  $\text{FePO}_4$  through a low-temperature hydrothermal reaction. The  $\text{FePO}_4$  nanosheets were formed and then assembled into  $\text{FePO}_4$  microspheres under coordination between urea and  $\text{Fe}^{3+}$ . The second step was to prepare  $\text{LiFePO}_4/\text{C}$  using beta-cyclodextrin as a carbon material via a carbothermal process in a hydrogen-argon mixture (95% Ar+5%  $\text{H}_2$ ). In the initial stage, hydrogen gradually seeped into the  $\text{FePO}_4$ , and the amorphous carbon was constantly formed in a tube furnace at a heating rate of  $5\text{ }^\circ\text{C min}^{-1}$ . Then,  $\text{Fe}^{3+}$  was reduced to  $\text{Fe}^{2+}$ , while  $\text{Li}^+$  was inserted into the electron hole as the temperature increased to the  $\text{FePO}_4$  reduction temperature. Then, the carbon layer disintegrated from the cyclodextrin coating on the surface of  $\text{LiFePO}_4$ . Finally, the carbon-coated  $\text{LiFePO}_4/\text{C}$  with intact crystallites was synthesized during the process with a cooling rate of  $3.5\text{ }^\circ\text{C min}^{-1}$ .



**Scheme 1.** The preparation process of  $\text{LiFePO}_4/\text{C}$

The electrochemical tests of the  $\text{LiFePO}_4/\text{C}$  and  $\text{LiFePO}_4$  powder were examined by testing half coin cells. To further explore the electrochemical performance of the carbon-coated  $\text{LiFePO}_4/\text{C}$  composite, the CV and constant current charge/discharge were tested. As shown in Fig. 5a, the cyclic voltammograms of the  $\text{LiFePO}_4/\text{C}$  cathode at a scan rate of  $0.4 \text{ mV s}^{-1}$  reveal a single-electron reaction mechanism. The good overlap of redox peaks during the three cycles indicates that electrochemical reversibility is established in the initial cycle. Fig. 5b shows the charge/discharge plots at various rates from 0.1C rate to 5C. The specific discharge capacity of the  $\text{LiFePO}_4/\text{C}$  cathode reaches  $146 \text{ mAh g}^{-1}$  at 0.1C rate and  $115 \text{ mAh g}^{-1}$  at 1C rate. The rate performance of the  $\text{LiFePO}_4/\text{C}$  and  $\text{LiFePO}_4$  electrodes is shown in Fig. 5c. The specific discharge capacity of  $\text{LiFePO}_4$  and  $\text{LiFePO}_4/\text{C}$  drop sharply at the 1C rate and 5C rate, respectively. The results demonstrate that the rate performance of the carbon-coated  $\text{LiFePO}_4/\text{C}$  is superior to pure  $\text{LiFePO}_4$ . However, the specific discharge capacity can recover completely when the discharge rate returns to the 0.1C rate, revealing that  $\text{LiFePO}_4$  and  $\text{LiFePO}_4/\text{C}$  have good structural stability and good electrochemical reversibility. To evaluate the cycling performance of  $\text{LiFePO}_4$  and  $\text{LiFePO}_4/\text{C}$ , 50 full charge/discharge cycles at a constant 0.5C rate were performed, as shown in Fig. 5d. The cyclability of the  $\text{LiFePO}_4$  and  $\text{LiFePO}_4/\text{C}$  cathodes was very stable during several cycles, and the specific discharge capacity of  $\text{LiFePO}_4/\text{C}$  did not tend to decline. The as-prepared  $\text{LiFePO}_4/\text{C}$  exhibited a common specific discharge capacity, an excellent rate performance and a stable cycling stability owing to the electronic conductivity of carbon, which was calcined from beta-cyclodextrin with a high content of residual carbon. Additionally, the electrochemical performance of the  $\text{LiFePO}_4/\text{C}$  cathode material prepared by our method is superior to those of  $\text{LiFePO}_4/\text{C}$  powders obtained via hydro/solvothermal, sol-gel, microwave synthesis and co-precipitation methods[10, 26, 30-32].

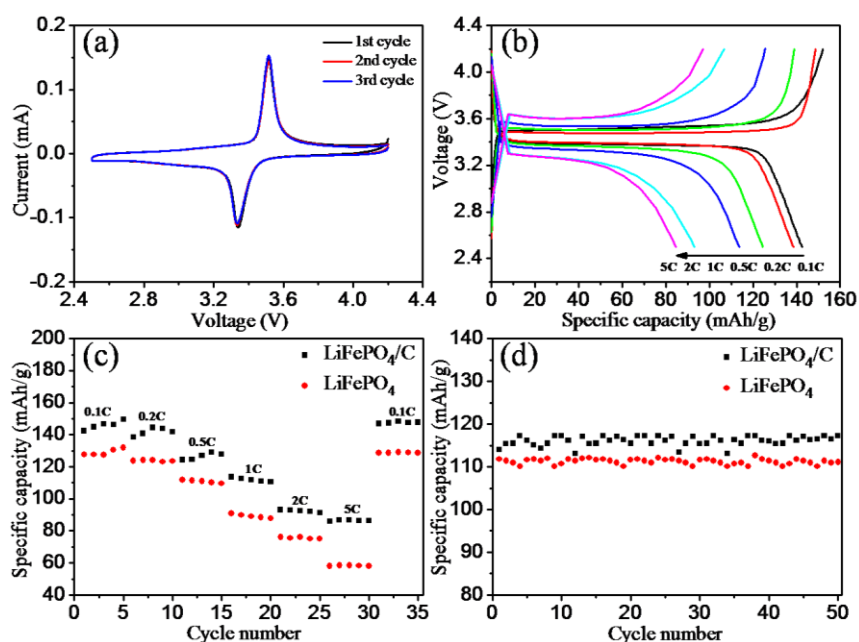


**Figure 5.** (a) Cyclic voltammogram of the  $\text{LiFePO}_4/\text{C}$  cathode at a scan rate of  $0.4 \text{ mV s}^{-1}$ ; (b) Charge and discharge profiles for  $\text{LiFePO}_4/\text{C}$  at various rates; (c) Rate performance of  $\text{LiFePO}_4$  and  $\text{LiFePO}_4/\text{C}$  at different discharge rates; (d) Cycle performance of  $\text{LiFePO}_4$  and  $\text{LiFePO}_4/\text{C}$  at 0.5C rate

The electrochemical impedance spectroscopy spectra (EIS) of  $\text{LiFePO}_4/\text{C}$  and  $\text{LiFePO}_4$  are shown in Fig.6. The high-frequency intercept of the diameter of the semicircle refers to the charge transfer resistance ( $R_{ct}$ ).  $R_{ct}$  relates closely to the electrochemical reaction at the cathode-electrolyte interface, revealing the charge transfer resistance in the cathode-electrolyte interface. Clearly, the charge transfer resistance decreases from  $320\ \Omega$  in  $\text{LiFePO}_4$  to  $180\ \Omega$  in  $\text{LiFePO}_4/\text{C}$ , indicating the carbon formed from the decomposition of beta-cyclodextrin could enhance the electronic conductivity, which would optimize the rate performance of  $\text{LiFePO}_4/\text{C}$  by improving the electronic conductivity. The sloped lines at the low frequencies correspond to the Warburg impedance ( $Z_w$ ), which is related to the lithium-ion diffusion in the electrodes.

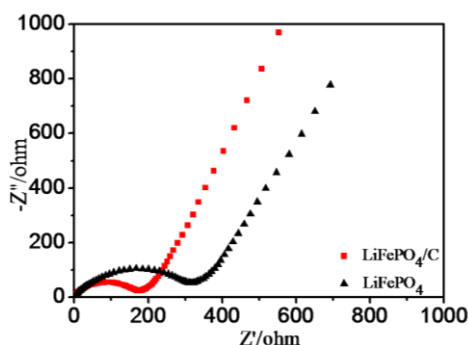


**Figure 6.** Impedance spectroscopy spectra of  $\text{LiFePO}_4/\text{C}$  and  $\text{LiFePO}_4$

#### 4. CONCLUSION

The morphology and electrochemical properties of the  $\text{LiFePO}_4/\text{C}$  cathode material synthesized via a carbothermal method based on beta-cyclodextrin as a carbon source were investigated. The  $\text{LiFePO}_4/\text{C}$  microspheres with diameters of  $5\text{-}10\ \mu\text{m}$  were aggregated by nanoplates after the carbothermal reduction, and their tap density reached as high as  $1.3\ \text{g cm}^{-3}$ . The surface of the  $\text{LiFePO}_4/\text{C}$  particles was coated with an amorphous carbon layer approximately  $3\ \text{nm}$  thick, which was the key parameter for increasing the electrical conductivity and optimizing the electrochemical performance. The unique structure and morphology contribute to the excellent rate performance and cycling stability of the  $\text{LiFePO}_4/\text{C}$  cathode material.

#### ACKNOWLEDGEMENTS

This work was fanatical supported by the National Natural Science Foundation of China (Grant No. 21276286 and No. 21476268) and the Open-End Fund for Valuable and Precision Instruments of Central South University (CSUZC201622).

#### References

1. G. Q. Xu, H. N. He, H. Wan, R. H. Liu, X. G. Zeng, D. Sun, X. B. Huang and H. Y. Wang, *J. Appl. Electrochem.*, 46 (2016) 879.

2. S. Wi, S. Nam, Y. Oh, J. Kim, H. Choi, S. Hong, S. Byun, S. Kang, D. J. Choi, K. Ahn, Y. Kim and B. Park, *J. Nanopart. Res.*, 14 (2012) 1327.
3. P. Gibot, M. Casas-Cabanas, L. Laffont, S. Levasseur, P. Carlach, S. Hamelet, J.M. Tarascon and C. Masquelier, *Nature. Mat.*, 7 (2008) 741.
4. Y. S. Kim, S. Cho, Y. K. Ahn, Z. Yin, D. J. You, H. Kim, Y. Piao and J. Yoo, *Chem-Eur. J.*, (2017).
5. Y. S. Hu, Y. G. Guo, R. Dominko, M. Gaberscek, J. Jamnik and J. Maier, *Adv. Mat.*, 19 (2007) 1963.
6. C. Hu, H. Yi, H. Fang, B. Yang, Y. Yao, W. Ma, and Y. Dai, *Int. J. Electrochem. Sci.*, 5 (2010) 1457.
7. F. Di Lupo, G. Meligrana, C. Gerbaldi, S. Bodoardo and N. Penazzi, *Electrochim. Acta*, 156 (2015) 188.
8. S. W. Oh, S. T. Myung, S. M. Oh, K. H. Oh, K. Amine, B. Scrosati and Y. K. Sun, *Adv. Mat.*, 22 (2010) 4842.
9. J. Zhao, J. He, J. Zhou, Y. Guo, T. Wang, S. Wu, X. Ding, R. Huang and H. Xue, *J. Phys. Chem. C.*, 115 (2011) 2888.
10. C. Sun, S. Rajasekhara, J. B. Goodenough and F. Zhou, *J. Am. Chem. Soc.*, 133 (2011) 2132.
11. J. Su, X. L. Wu, C. P. Yang, J. S. Lee, J. Kim and Y. G. Guo, *J. Phys. Chem. C.*, 116 (2012) 5019.
12. L. Wang, H. Liu, Z. Tang, L. Ma and X. Zhang, *J. Power. Sources*, 204 (2012) 197.
13. R. Chen, J. Lai, Y. Li, M. Cao, S. Chen and F. Wu, *RSC. Adv.*, 6 (2016) 103364.
14. S. h. Wu, J. J. Shiu and J. Y. Lin, *J. Power. Sources*, 196 (2011) 6676.
15. C. Hu, H. Yi, H. Fang, B. Yang, Y. Yao, W. Ma and Y. Dai, *Mater. Lett.*, 65 (2011) 1323.
16. Y. Qiu, Y. Geng, J. Yu and X. Zuo, *J. Mater. Sci.*, 49 (2013) 504.
17. J. Gustafsson, L. Ciofica and J. Peltonen, *Polymer*, 44 (2003) 661.
18. S. T. Jackson and R. G. Nuzzo, *Appl. Surf. Sci.*, 90(1995) 195.
19. Y. Wang, Y. Wang, E. Hosono, K. Wang and H. Zhou, *Angew. Chem.*, 47 (2008) 7461.
20. N. Yamakawa, M. Jiang, B. Key and C. P. Grey, *J. Am. Chem. Soc.*, 131 (2009) 10525.
21. S. Sun, H. Zeng, D. B. Robinson, S. Raoux, P. M. Rice, S. X. Wang and G. Li, *J. Am. Chem. Soc.*, 126 (2004) 273.
22. J. Qian, M. Zhou, Y. Cao, X. Ai and H. Yang, *J. Phys. Chem. C.*, 114 (2010) 3477.
23. S.W. Oh, H. J. Bang, S. T. Myung, Y. C. Bae, S. M. Lee and Y. K. Sun, *J. Electrochem. Soc.*, 155 (2008) A414.
24. M.S. Dresselhaus, A. Jorio, M. Hofmann, G. Dresselhaus and R. Saito, *Nano. Lett.*, 10 (2010) 751.
25. T. Wang, Y. Wang, Y. N. Wu, L. Zhou, Y. Jin, W. M. Liu, J. Huang, X. Fang and X. C. Tang, *Int. J. Electrochem. Sci.*, 12 (2017) 975.
26. Q. H. Zhang, Y. Q. Feng and S. L. Da, *Chromatographia*, 50 (1999) 654.
27. J. L. Mohanan, I. U. Arachchige and S. L. Brock, *Science*, 307(2005) 397.
28. Y. Jin, X. C. Tang and H. Y. Wang, *RSC. Adv.*, 6 (2016) 75602.
29. R. Saroha and A. K. Panwar, *J. Phys. D. Appl. Phys.*, 50 (2017) 25.
30. K. F. Hsu, S. Y. Tsay and B. J. Hwang, *J. Mater. Chem.*, 14 (2004) 2690.
31. M. Higuchi, K. Katayama, Y. Azuma, M. Yukawa and M. Suhara, *J. Power. Sources*, 119-121 (2003) 258.
32. C. W. Ong, Y. K. Lin and J. S. Chen, *J. Electrochem. Soc.*, 154 (2007) A527.